

www.acsanm.org Article

# Laser-Induced Graphene Decorated with Platinum Nanoparticles for Electrochemical Analysis of Saliva

Robert G. Hjort, Cícero C. Pola, Raquel R. A. Soares, Jemima Opare-Addo, Emily A. Smith, Jonathan C. Claussen,\* and Carmen L. Gomes\*



Cite This: ACS Appl. Nano Mater. 2023, 6, 20801-20811



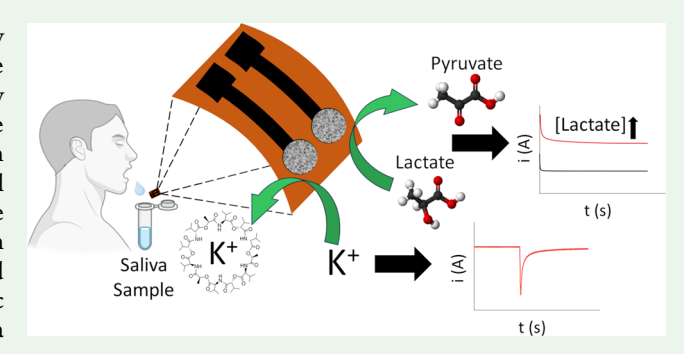
**ACCESS** 

III Metrics & More

Article Recommendations

s Supporting Information

ABSTRACT: Saliva-based sensors are becoming increasingly important in medical diagnostics and sports medicine due to the plethora of biomedically relevant analytes found endogenously within the fluid and to the inherently noninvasive nature of the sensing protocols. Salivary lactate and potassium have been shown to be key indicators for monitoring fatigue, hydration, and overall health, and frequent monitoring is crucial for preventative treatment strategies. Low-cost test strip sensors combined with saliva swab sampling could enable such frequent monitoring, and to this end, we developed amperometric lactate and coulometric potassium test strip sensors using laser-induced graphene (LIG), a low-cost scalable fabrication method for graphene sensor develop-



ment. To increase the sensitivity of the sensors, platinum nanoparticles (nPt) were deposited on the LIG surface by using a facile electroless deposition method. Subsequently, a redox mediator with the enzyme lactate oxidase was used for lactate sensing, while a polymer-based ion-selective membrane was used for potassium sensing. The lactate biosensor displayed a sensitivity of  $33.3 \pm 0.9 \,\mu\text{A}$  mM<sup>-1</sup> cm<sup>-2</sup> and a limit of detection (LOD) of  $0.10 \pm 0.06$  mM, while the potassium sensor exhibited a sensitivity of  $168.2 \,\mu\text{C}$  dec<sup>-1</sup> and a signal-to-noise ratio (S/N) of  $193.3 \pm 56.2$ . Both sensors were capable of selectively sensing within the physiologically relevant range with real pooled saliva samples. Such sensing results demonstrate the potential of nPt-LIG for point-of-care biosensors for personalized health and athletic performance monitoring.

KEYWORDS: biosensor, diagnostics, nano materials, graphene, metabolites, electrolytes

# **■ INTRODUCTION**

The nascent and burgeoning fields of precision and personalized medicine are enabled by integrating health monitoring and diagnostics into everyday life. Such routine testing will require sensor systems that are not only capable of laboratory-grade accuracy and sensitivity but also affordable, easy-to-use, and noninvasive so that they can be widely adopted. Saliva offers a promising biological fluid for precision health monitoring and diagnostics due to the noninvasive nature of the sampling (no need for a blood draw at a laboratory or a fingerstick at home) and due to the abundance of medically relevant electrolytes, proteins, and immunoglobulins found within saliva.<sup>2,3</sup> Saliva can be extracted at almost any time and can be easily collected and stored as opposed to other biological fluids that can be noninvasively extracted (e.g., sweat, tears, and urine) but require special collection procedures or are released only intermittently (e.g., when one is sweating or when one needs to micturate). Saliva can also be used for monitoring infections; for example, we recently demonstrated how a saliva-based immunosensor could be used to detect COVID-19 infection, a sensor test that circumvents the need for uncomfortable nasal swabs.

Frequent monitoring of salivary lactate and potassium is of particular interest for precision health and sports medicine. Lactate is a well-known metabolic waste product that increases when adenosine triphosphate (ATP) and oxygen demand exceeds supply, such as during exercise. Continuous monitoring of blood lactate can give real-time information for training and performance evaluation for athletes or others engaged in strenuous physical training, such as in the military. There is also a clinical diagnostics interest to accurately measure lactate levels due to the association with several disorders (i.e., heart failure, hereditary disorders, and respiratory insufficiency). Moreover, recent research has demonstrated that salivary lactate displayed a correlation with blood lactate levels during exercise and hence has the potential to be used for monitoring fatigue levels. Although

Received: August 14, 2023 Revised: October 23, 2023 Accepted: October 25, 2023 Published: November 15, 2023





salivary lactate levels (~0.3 mM at rest and up to ~4.0 mM during exercise)8,9 have been reported at lower levels than blood lactate, consequently requiring more sensitive devices, the noninvasive collection of saliva is a big appeal for its use in diagnostics. Potassium, along with sodium, is one of the major electrolytes required to maintain a proper water balance. Clinical studies show that increasing dietary potassium can lead to lower blood pressure in both normotensive and hypertensive populations. 10 High potassium intake has also been shown to reduce the risk of strokes and kidney stones and slow the progression of renal disease.<sup>11</sup> Recent research has also demonstrated consistent correlations between salivary potassium and serum osmolality levels and showed that monitoring salivary potassium could be used to diagnose dehydration as well as diseases such as chronic kidney disease. 12 A recent study reports investigating saliva as a diagnostic fluid including the monitoring of the differences between day-to-day variability, time of collection, and site of collection.<sup>13</sup> The mean potassium levels for the right and left vestibulum were 23.2 and 23.6 mM, respectively, with a 14.4% difference in day-to-day means. Mid-morning saliva samples were shown to have 15-30% lower levels than early-morning saliva samples. Another group reported the effect of incremental exercise and showed that salivary potassium at the beginning was approximately 25 mM and decreased to nearly 15 mM after 300 min.<sup>14</sup>

Current methods to detect both potassium and lactate are generally not conducive to the frequent, low-cost, at-home, and in-field testing that precision health requires. Centralized laboratories can accurately detect lactate using a variety of methods including chromatography and enzyme-based spectrophotometric or colorimetric methods. 15 While these methods are sensitive and selective, they require trained personnel and expensive equipment hindering the ability for continuous point-of-care monitoring. Industry has started offering portable electrochemical lactate sensors (e.g., the Lactate Plus by Nova Biomedical) that circumvent these drawbacks, but they require the user to perform a fingerpick to measure lactate blood levels. Current commercial lactate sensors are not designed for salivary lactate sensing and use uncomfortable/painful methods to draw blood for testing that are not conducive to wide-scale adoption. Likewise, potassium is generally measured in laboratory settings with liquid junction potassium ion-selective electrodes (ISEs). Such liquid junction ISEs require regular maintenance and conditioning to maintain their accuracy and reliability including periodically replenishing the electrolyte solution of the reference electrode and cleaning/replacing the liquid junction itself. 16 Potentiometric solid-contact ion-selective electrodes (ISEs) have shown promise for point-of-care monitoring of salivary electrolytes by circumventing the regular maintenance and conditioning required by liquid junction ISEs. 17-19 Moreover, these so-called solid-contact ISEs typically operate in a wide range of ion concentrations with a low limit of detection (LOD) with the added benefit of facile miniaturization and less complexity and cost than liquid junction ISEs. However, issues with signal stability and reproducibility of the standard potential  $(E^0)$  require frequent recalibration, which could limit the use in complex sample analysis. 16,20 Constantpotential coulometry is a recently proposed alternative<sup>21</sup> to traditional potentiometric ISEs for ion detection and may overcome some limitations associated with ISEs. Since the electrode potential is held constant, any change in the primary

ion activity causes a reducing/oxidizing current to flow due to the potential change at the membrane/sample interface and solid contact. The current can be integrated to obtain the cumulated charge (Q), which has a linear relationship with the logarithm of the primary ion activity.<sup>22</sup>

Material choice for the underlying electrode has a significant effect on the performance of subsequent biosensors. Graphenebased electrodes offer a promising solution for developing effective salivary lactate and potassium electrochemical sensors due to their high surface area (2630 m<sup>2</sup> g<sup>-1</sup>), mechanical strength (Young's modulus ~1100 GPa), electrical conductivity (~64 mS cm<sup>-1</sup>), chemical stability, biocompatibility, and tunable properties. However, the complexity and cost associated with their fabrication have impeded their implementation into single-use test strip sensors. Even highyield mechanical and/or chemical exfoliation of graphene from graphite followed by solution-phase printing of electrodes can be costly due to the complexity of ink formulation and the need for postprint annealing requirements. 26,27 However, laserinduced graphene (LIG) circumvents the need to exfoliate graphene from graphite or to create a solution-phase graphene ink by converting sp<sup>3</sup> carbon found in carbon-rich substrates, such as polyimide into conductive sp<sup>2</sup>-hybridized carbon found in graphene through a laser scribing technique. <sup>28</sup> Moreover, we have demonstrated that the surface area and wettability of the LIG can be tuned to greatly improve the sensitivity of electrochemical enzymatic biosensors (detection limits down to the picomolar range) and reduce the water layer buildup between the ISE membrane and the electrode, which improves the accuracy of the sensor readings.<sup>29-31</sup> LIG has also been used in a wide variety of electrochemical sensing applications including in food safety,<sup>32</sup> environmental monitoring, wearable health sensors,<sup>33</sup> and even for urinary potassium<sup>34</sup> and salivary lactate sensing.<sup>35</sup> However, a LIG electrochemical sensor system capable of monitoring metabolites and electrolytes, such as lactate and potassium, in actual human pooled saliva samples has not been previously explored. Such a system would allow for facile dual monitoring of fatigue and dehydration through a noninvasive technique.

In this work, LIG was developed into an enzymatic lactate biosensor and a constant-potential coulometric potassium sensor. The LIG was fabricated on polyimide (PI, Kapton) in a one-step lasing process with a CO<sub>2</sub> laser ( $\lambda = 10.6 \mu m$ ) that did not require reagents or postfabrication annealing. An electroless deposition method was used to deposit platinum nanoparticles on the surface of the LIG and confirmed using Xray photoelectron spectroscopy (XPS) and energy-dispersive X-ray spectroscopy (EDS). Lactate oxidase (LOx) or a polyvinyl chloride (PVC)-based ion-selective membrane was coated on the surface of the LIG to form lactate and potassium sensors, respectively. After calibration and selectivity studies, each sensor was calibrated in samples with diluted pooled saliva. Flexibility studies were also performed to evaluate the ability of the sensors to operate under stresses caused by bending such as those that would be encountered by implanted oral sensors. Hence, the results obtained in this study suggest that LIG with platinum nanoparticles can act as a simple method for scalable production of noninvasive salivary health sensors.

#### METHODS AND MATERIALS

Materials. Chloroplatinic acid hexahydrate (≥37.5%), 10× phosphate-buffered saline (PBS), ammonium hydroxide (28–30%

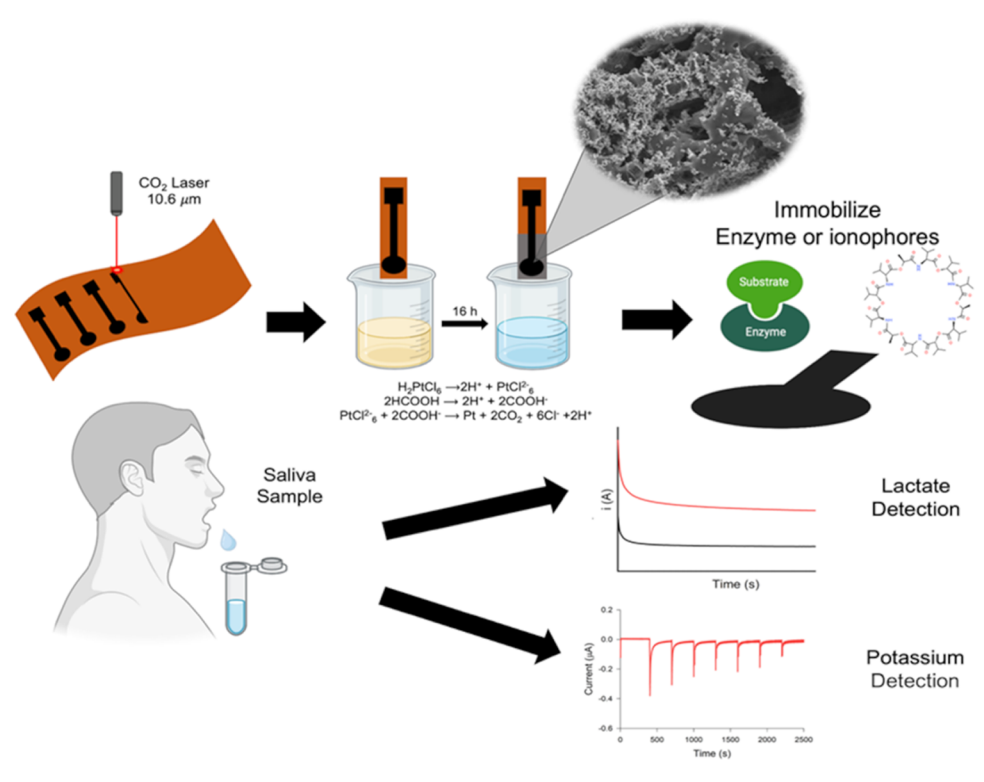


Figure 1. Schematic of LIG fabrication and electroless platinum deposition followed by functionalization with enzymes or ionophores. Saliva samples were then analyzed for lactate using amperometry, where a high concentration (red curve) generates a larger current relative to a lower concentration (black curve). Potassium detection was performed using constant-potential coulometry that uses cumulated charge during current pulses for potassium quantification.

(w/w)), potassium chloride, and sodium l-lactate ( $\geq$ 98%) were purchased from Fisher Scientific (Massachusetts). Tetrathiafulvalene (TTF, 97%), formic acid, chitosan (75–85% deacetylated), calcium chloride, magnesium chloride, sodium chloride, and all chemicals used for the ion-selective membrane were purchased from Millipore Sigma (Darmstadt, Germany). Lactate oxidase was purchased from AG Scientific (California). A polyimide (PI) film with 5 mil thickness was purchased from McMaster-Carr (Ohio). Solutions were prepared using deionized (DI) water with ~18.2 M $\Omega$  cm resistivity, and all chemicals were analytical grade.

LIG Fabrication and Platinum Deposition. LIG was fabricated with a 75 W M2 Fusion Epilog (Colorado) CO<sub>2</sub> laser. Polyimide was cleaned with ethanol, dried with high-purity nitrogen, and treated with the laser in raster mode at 7% speed, 6% power, and 1200 DPI in air  $(23 \pm 1 \, ^{\circ}\text{C})$  at a +2 mm offset from the focal point. The electrodes were passivated with a fast-drying lacquer, leaving a working area of 3 mm. The electrode leads were coated with a conductive silver ink (Cl-1001, Engineering Materials Systems Inc., Ohio). Platinum deposition was done inside a fume hood following our previously published method<sup>36</sup> based on the reduction of chloroplatinic acid by formic acid at room temperature. Briefly, 180 mg of chloroplatinic acid was added to 30 mL of formic acid and DI water (1:9), and the pH was adjusted to 2.5 with ammonium hydroxide. The LIG electrodes were submerged in the solution, and beakers were covered with parafilm for 16 h until the solution turned from yellow to clear. Once the reaction was complete, the electrodes were rinsed with DI water and allowed to air-dry in a fume hood.

**LIG Functionalization.** *LOx Biosensors.* The platinum LIG was drop-coated twice with 0.02 M TTF in acetone/ethanol (1:9), followed by 60 mg mL $^{-1}$  lactate oxidase (LOx). Finally, 0.6% (w/v) chitosan (75–85% deacetylated) in 0.1% (v/v) acetic acid was drop-coated on the sensor and stored at 4 °C for 24 h. Each coating was drop-coated using a pipette containing 3  $\mu$ L and allowed to dry for approximately 45 min.

Potassium Ion Sensors. Two 3 µL applications of 0.02 M TTF in acetone/ethanol (1:9) were applied to the Pt-LIG. Inside a fume

hood, a mixture of 1.9 mg of valinomycin, 0.6 mg of potassium tetrakis(4-chlorophenyl) borate, 58.4 mg of polyvinyl chloride (PVC), and 127.7  $\mu$ L of dioctyl sebacate (DOS) was dissolved in 1 mL of tetrahydrofuran (THF, anhydrous,  $\geq$ 99.9%) and vortexed for approximately 1 min until homogenized. A 3  $\mu$ L application of the membrane was drop-coated on top of the TTF layer and allowed to dry overnight in a fume hood. The electrodes were conditioned in 0.1 M KCl for 48 h before testing. Ionic strength was calculated using eq S1, and the extended Debye—Hückel approximation (eq S2) was used to calculate all activity coefficients.

Material Characterization. Scanning electron microscopy (SEM) images were taken using a FEI Teneo LoVac field emission SEM (FESEM) at an accelerating voltage of 1 kV and a beam current of 25 pA. Raman spectroscopy measurements were performed using a Horiba XploRA Plus confocal Raman microscope with a 532 nm laser operating at 1.2 mW and a  $50\times$  objective (0.5 NA). The spectra were collected from 600 to 3000 cm<sup>-1</sup> with 600 grooves mm<sup>-1</sup> grating. Six Raman spectra were collected at six randomly selected locations, and each Raman spectrum was collected with a 30 s acquisition and three accumulations. All Raman peaks in each spectrum were fitted to a Lorentzian function in Igor Pro 6.37. The  $I_{\rm D}/I_{\rm G}$  and  $I_{\rm 2D}/I_{\rm G}$  ratios were calculated from the fitting results. X-ray photoelectron spectroscopy (XPS) analysis was performed using a Kratos Amicus/ESCA 3400 instrument and irradiated with 240 W unmonochromated Mg Ka Xrays. The 3D optical profile image was captured using an S-neox system from Sensofar with a TU Plan Fluor 20×.0.45a objective from Nikon to obtain fast, noninvasive assessment sample geometry. A series of 100 nm steps through the vertical range of the sample height in combination with confocal-based exclusion of the out-of-focus light allows a series of vertical images to be collected and used to reconstruct the three-dimensional image of the sample with a high degree of accuracy.

**Electrochemical Characterization.** Galvanostatic charge—discharge (CC) experiments were performed on a CH Instruments (Texas) electrochemical analyzer model CHI7018E. Cyclic voltammetry (CV), amperometric *i*—t measurements, and constant-potential

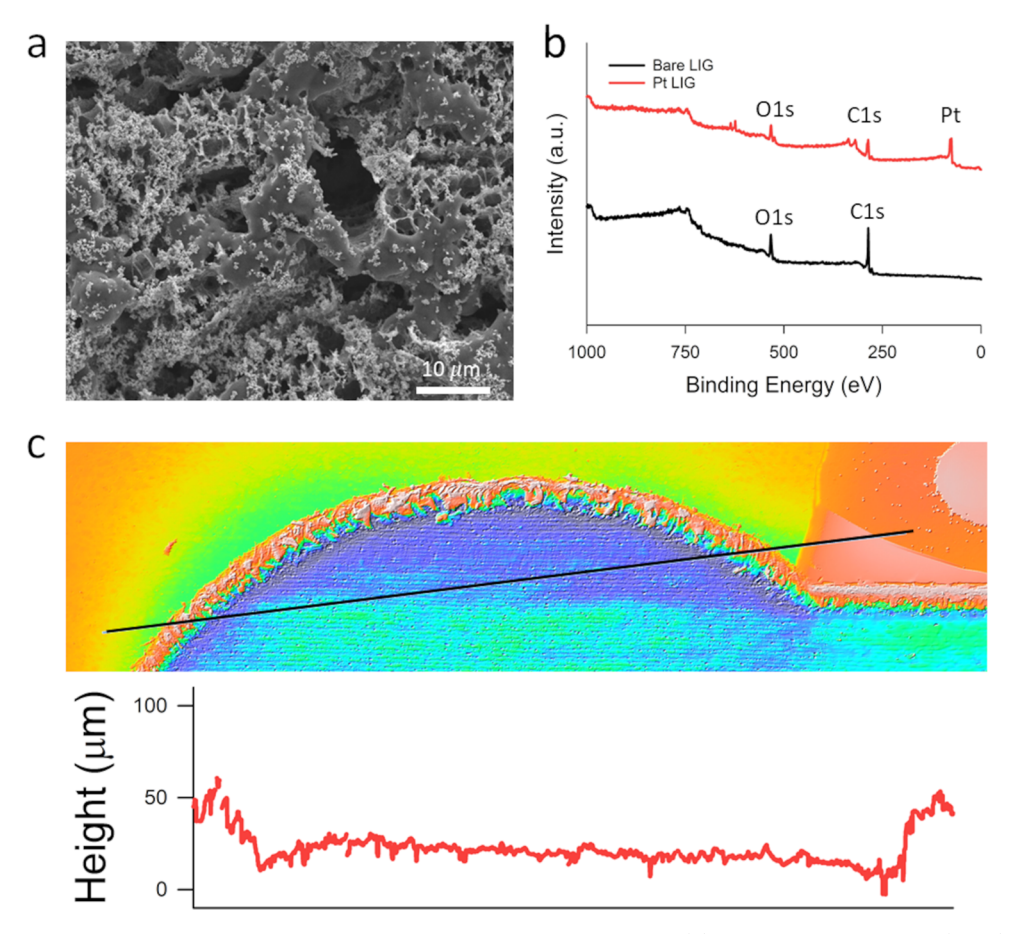


Figure 2. (a) SEM image showing platinum nanoparticles on the porous surface of the LIG. (b) XPS survey of bare LIG (black) showing typical O 1s and C 1s peaks and platinum LIG (red) showing reduced O 1s and C 1s peaks with an additional Pt peak. (c) 3D microscopy image of a bare LIG electrode using an S-neox system from Sensofar showing the 3D structure of the material with an approximate average height of  $\sim$ 25  $\mu$ m.

coulometry were performed on a PalmSens 4 potentiostat (the Netherlands). For all experiments, an external Ag/AgCl electrode (3 M KCl liquid junction) functioned as the reference electrode, and a platinum wire electrode (99.95% Pt, 0.5 mm diameter) functioned as the counter electrode.

CV analysis was performed in 5 mM ferro/ferricyanide in 0.1 M KCl at 10, 20, 40, 60, 80, and 100 mV s $^{-1}$  from -0.4 to 0.8 V, and electroactive surface area (ESA) calculations were made with eq S3. CC measurements were performed using 1 M  $\rm H_2SO_4$  and seven current densities from 15 to 45  $\mu\rm A$  cm $^{-2}$  for bare LIG and 6–20 mA cm $^{-2}$  for platinum LIG. Specific areal capacitance (CA, mF cm $^{-2}$ ) was calculated using the CC curves and eq S4.

Amperometric i-t curves were performed in  $10\times$  PBS (pH = 7.4) at physiologically relevant levels  $^{37}$  of lactate concentrations in saliva (0.4–1.5 mM). Scans were performed by applying +0.3 V for 60 s. Coulometric detection of potassium was completed by performing amperometric i-t curves from physiologically relevant levels  $10^{-1.95}$  to  $10^{-1.65}$  M KCl in 0.05 log steps with a background of  $10^{-2}$  M KCl. During the experiments, an applied potential of 0 V was used with 300 s between KCl additions, and a stir bar operated at 300 rpm. Interference of ascorbic acid, uric acid, and glucose was tested for the lactate biosensor in  $10\times$  PBS, and  $Ca^{2+}$ ,  $Mg^{2+}$ , and  $Na^+$  were tested for the F\* sensor with a background of 15 mM KCl. The functionality of the potassium sensors was first confirmed in traditional potentiometric mode using a Ag/AgCl (3 M KCl) reference electrode.

**Pooled Saliva Analysis.** Pooled human saliva samples were provided by the Research and Education in Disease Diagnostics and Intervention (REDDI) Lab at Clemson University. Samples for the lactate biosensor were diluted to 10% saliva with 10× PBS, and samples for the potassium sensor were diluted to 10% saliva with DI

water. Calibrations were performed using the parameters mentioned above from 0.4 to 2.5 mM lactate and from  $\sim$ 10 to 25 mM potassium.

**Data Analysis.** All measurements were made in triplicate and were reported as the mean  $\pm$  standard deviation. One-way analysis of variance (ANOVA) and Student's t-test were performed with JMP Pro v.15 statistical software (SAS Institute, Cary, NC) using a significance level of 0.05. All figures were generated in SigmaPlot 14 (Systat Software Inc., San Jose, CA).

#### RESULTS AND DISCUSSION

Biosensor Fabrication. Figure 1 shows the fabrication process that began by lasering the polyimide film under ambient conditions (air,  $23 \pm 1$  °C) using a CO<sub>2</sub> laser with a 10.6  $\mu$ m wavelength to produce LIG electrodes. Next, platinum nanoparticles (nPt) were formed on the LIG using the reduction of chloroplatinic acid  $(H_2PtCl_6)$  by formic acid (HCOOH) following our previous protocol.<sup>36</sup> Once the nPt-LIG was obtained, tetrathiafulvalene (TTF) was drop-coated on the surface of the LIG. Enzymes (lactate oxidase, LOx) or ionophores (valinomycin) were deposited on the surface to form sensors sensitive to lactate and potassium, respectively. LOx was embedded in a layer of chitosan to prevent leaching, while valinomycin was diluted in a poly(vinyl chloride) (PVC)-based membrane and drop-coated on the surface. Saliva samples were then analyzed for lactate concentration using amperometry and potassium concentration using constant-potential coulometry.

Material Characterization. Platinum (Pt), although more expensive than gold (Au) or silver (Ag), is commonly used due to

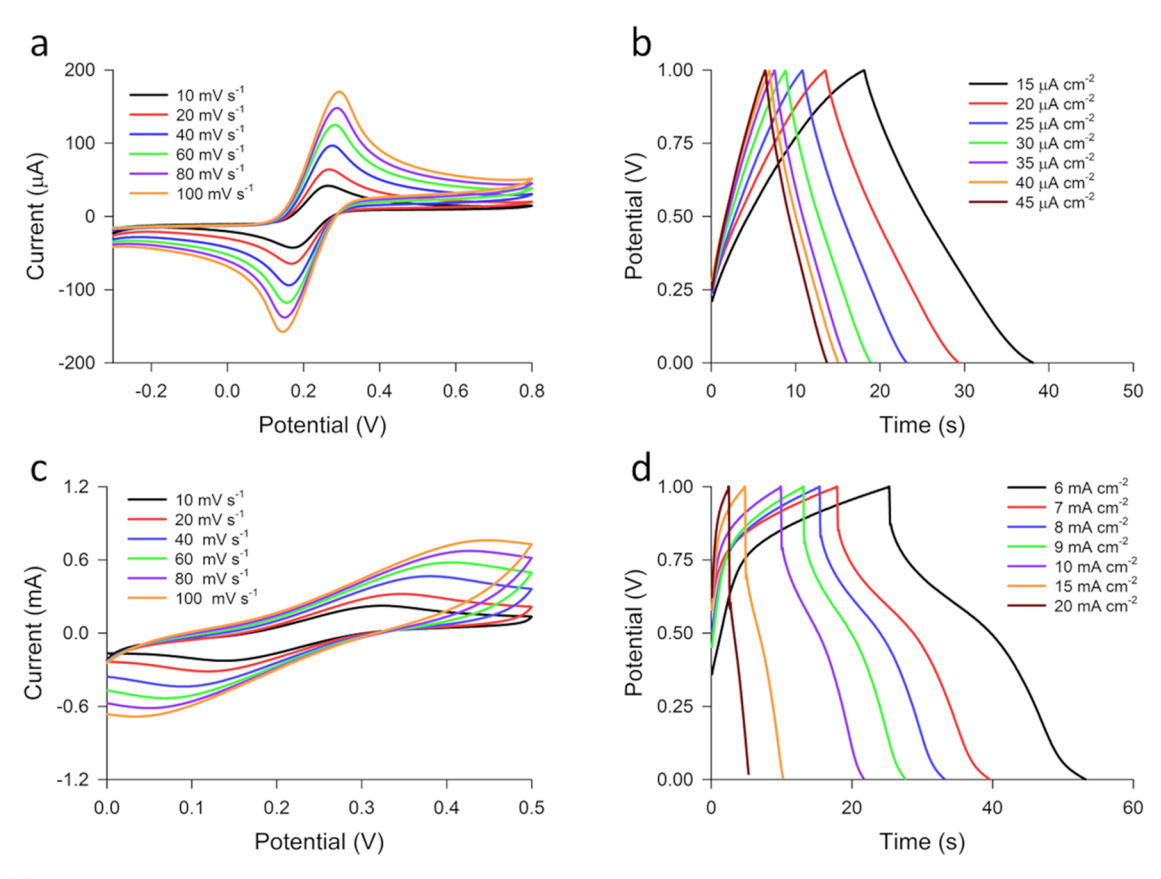


**Figure 3.** (a) CV scans for bare LIG in 5 mM ferri/ferrocyanide with 0.1 M KCl. Distinctive redox peaks are observed around 259.65 and 169.73 mV. (b) CC curves for bare LIG in 1 M  $_2$ SO<sub>4</sub> at seven current densities from 15 to 45  $\mu$ A cm<sup>-2</sup>. (c) CV scans for nPt-LIG in 5 mM ferri/ferrocyanide with 0.1 M KCl displaying a predominately capacitance current response when compared to bare LIG. (d) CC curves for nPt-LIG in 1 M  $_2$ SO<sub>4</sub> showing a higher capacitance compared to bare LIG at seven current densities from 6 to 20 mA cm<sup>-2</sup>.

several advantages including the unreactive nature with water, acids, and bases and the lack of oxidation in air. 38 Traditional methods such as electron beam lithography and chemical vapor deposition (CVD) techniques can be used to deposit nPt for sensors and fuel cells along with electroless and electrochemical deposition. Electroless deposition of platinum offers a simple method to produce nPt through the reduction of Pt from a salt solution onto an electrode surface. <sup>39</sup> In this study, formic acid was used to reduce Pt onto LIG using chloroplatinic acid, where the reaction speed and nPt density are highly dependent on the pH, as high H+ presence hinders reaction progress and leads to higher nPt density. Three pH levels (1.0, 2.5, and 4.0) were tested with a pH of 2.5, displaying the densest and most consistent coverage of nPt (Table S1). The morphology was studied by SEM, as shown in Figures 2a and S1a, where nPt growth can be seen on the LIG substrate. An SEM image of bare LIG and results from Raman spectroscopy are shown in Figure S2a,b, respectively. The Raman spectrum exhibited three characteristic peaks typical of graphene-based materials produced through CO<sub>2</sub> laser irradiation. These peaks correspond to the D, G, and 2D bands. The D peak, at approximately 1348 cm<sup>-1</sup>, implies the presence of structural defects or bent regions within the graphene structure. The G peak, at around 1587 cm<sup>-1</sup>, corresponds to the in-plane vibrations of sp<sup>2</sup> carbon atoms, and the 2D peak, located at roughly 2689 cm<sup>-1</sup>, indicates the stacking of graphene sheets. 40 The corresponding ratio  $I_{\rm D}/I_{\rm G}$  = 1.0  $\pm$ 0.1 indicates a high degree of graphene disorder, usually due to breaks in the translational symmetry, typical of porous LIG. 40 Additionally, the ratio  $I_{\rm 2D}/I_{\rm G}$  = 0.5  $\pm$  0.1 suggests that the graphene formed displays a multilayered structure. Surface elemental composition analysis was performed with XPS (Figure 2b) for bare LIG (black) and for platinum LIG (red), with both samples displaying peaks centered at approximately 286 and 533 eV attributed to C 1s and O 1s, respectively. 41 The platinum LIG has an additional doublet peak at

approximately 74 eV (low energy band) and 77 eV (high energy band) attributed to Pt  $4f_{7/2}$  and Pt  $4f_{5/2}$ , respectively  $^{42,43}$  (Figure S3). Deposition of nPt was further validated through energy-dispersive X-ray spectroscopy (EDS), shown in Figure S1b,c with the characteristic Pt M $\alpha$  peak at slightly over 2 keV.  $^{43,44}$  The average resulting mass percentage from EDS analysis was  $67.74\pm2.70\%$  Pt and  $32.26\pm0.40\%$  C, which is much higher than the electrochemical deposition of Pt (Figure S4, n=3). Figure 2c shows a 3D image of the Pt-LIG and the subsequent height profile, which resulted in a material thickness of  $\sim\!\!25~\mu m$ , which has been previously reported as the approximate thickness of LIG.  $^{28}$ 

**Electrochemical Characterization.** Metal nanoparticles are commonly used to improve the electrical and catalytic properties of electrode surfaces, improving the performance of subsequent biosensors.<sup>45</sup> Cyclic voltammetry (CV) was used to electrochemically characterize the bare LIG and nPt-LIG at different scan rates (10, 20, 40, 60, 80, and 100 mV s<sup>-1</sup>). For the bare LIG, distinct anodic and cathodic peaks are present at approximately 259.65 and 169.73 mV, respectively (Figure 3a), and increased linearly with the square root of the scan rate (Figure S5), suggesting an electrochemical system that is diffusion-governed. 46 The voltage peak-to-peak separation at 10 mV s<sup>-1</sup> was 89.92 mV, which is slightly higher than that of a reversible system ( $\Delta E_p$  < 60 mV). Simultaneously, the observed increase in the potential peak-to-peak separation indicates limitations in electron transfer. 46 Hence, current is controlled by a combination of mass transport and electron transfer, which discloses a quasi-reversible electrochemical system. 47 The electroactive surface area (ESA) was calculated using Randles-Sevcik theorem (eq S3) and resulted in an ESA

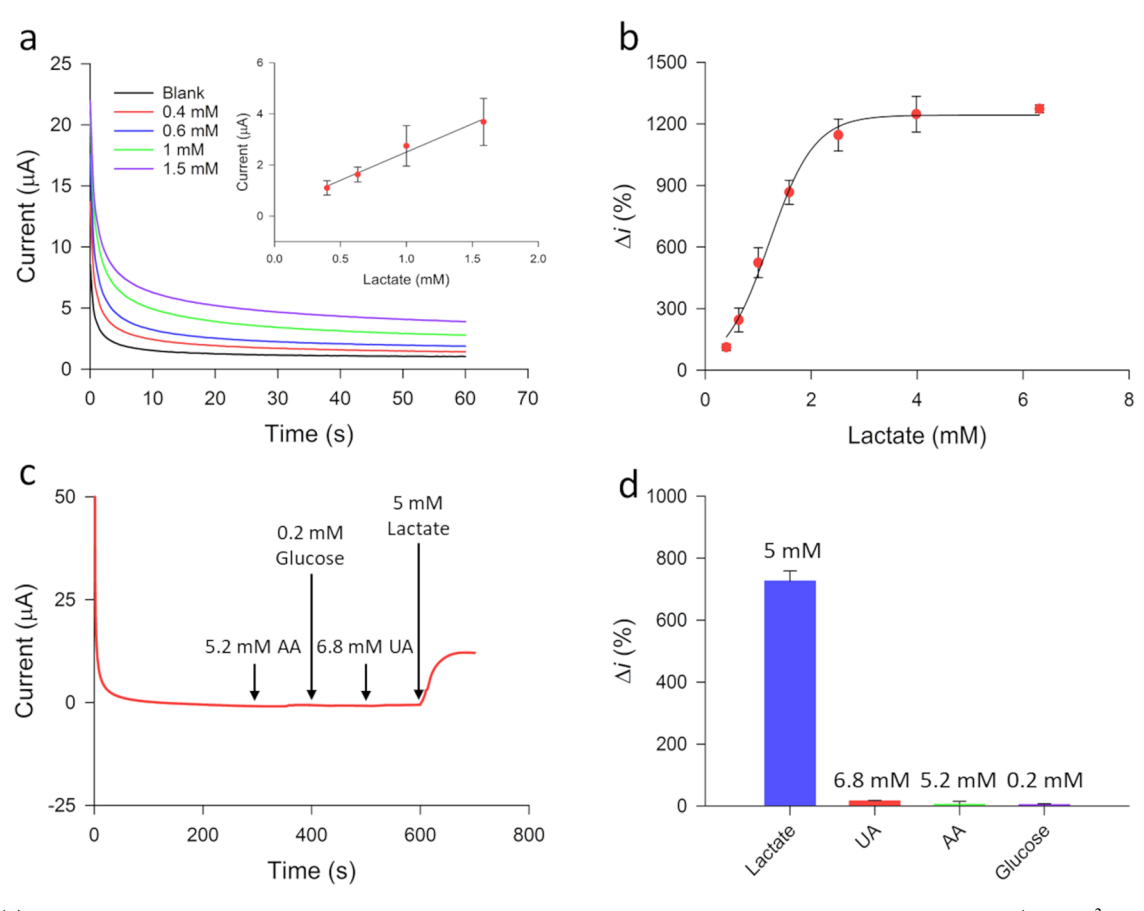
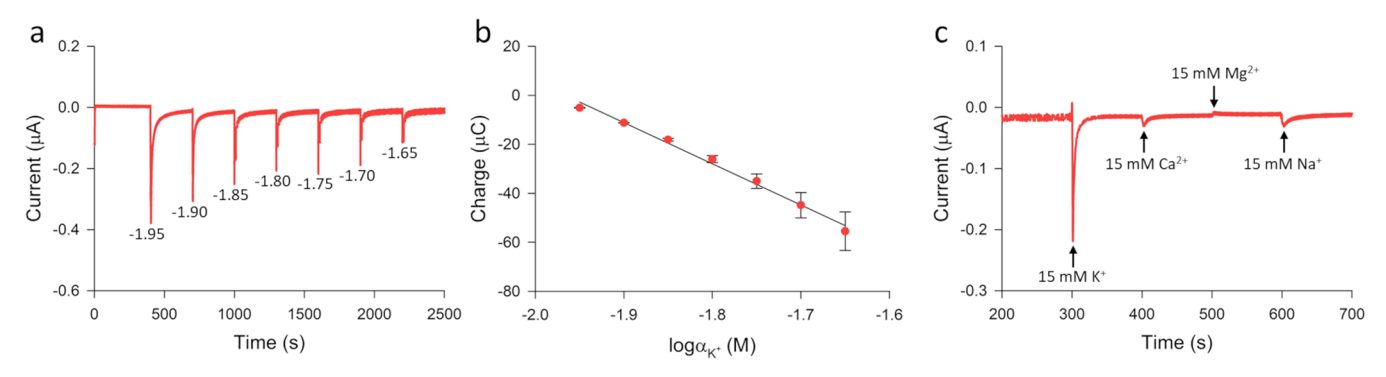


Figure 4. (a) Amperometric i-t curves for lactate sensing from 0.4 to 1.5 mM and the resulting linear calibration plot (inset,  $R^2 = 0.9798$ ). (b) Percent change in current relative to the baseline for 0.4–6.2 mM lactate showing signal saturation after 2.5 mM. (c) Real-time selectivity study showing negligible current change for 5.2 mM ascorbic acid (AA), 6.8 mM uric acid (UA), and 0.2 mM glucose followed by an addition of 5 mM lactate and a large current increase. (d) Percent change in current relative to the baseline signal for 5 mM lactate (blue), 6.8 mM AA (red), 5.2 mM UA (green), and 0.2 mM glucose (purple), with lactate displaying the largest change in current. Data represents mean  $\pm$  standard deviation (n = 3).

of  $16.92 \pm 0.75 \text{ mm}^2$ , 139.32% larger than the geometric area (7.07 mm<sup>2</sup>), which is a similar result to previously reported works with LIG electrodes.<sup>32,48</sup> The larger ESA compared to the geometric area is likely due to the porous nature of the 3D graphene structure, which increases the surface area and exposes more edge planes of the graphene to the redox solution, facilitating easier electron transfer. 49,50 CV scans for the nPt-LIG did not display apparent redox peaks and approached a quasi-square shape as a capacitance current appeared to dominate the reaction (Figure 3c). Galvanostatic charge-discharge curves in 1 M H<sub>2</sub>SO<sub>4</sub> were used to further study the capacitive response of both the bare LIG and nPt-LIG at various current densities of 15–45  $\mu$ A cm<sup>-2</sup> and 6–20 mA cm<sup>-2</sup>, respectively. The bare LIG (Figure 3b) had an average areal capacitance (CA) of 0.312 mF cm<sup>-2</sup>, which increased to 122.55 mF cm<sup>-2</sup> after platinum nanoparticle deposition (Figure 3d). The high capacitance of the LIG is likely due to the highly conductive 3D structure of the LIG, increasing the surface area and providing easy access for the electrolyte to form a Helmholtz layer.<sup>51</sup> These properties are likely increased with platinum nanoparticle deposition, leading to an increase in capacitance.

**Lactate Biosensor.** A lactate biosensor was developed with the nPt-LIG by first drop-coating the redox mediator TTF, which has been previously reported as a mediator for lactate biosensors. Furthermore, studies without TTF where dissolved oxygen species are the electron carriers resulted in

a negligible response to lactate. Once the TTF layer was dry, 60 mg mL<sup>-1</sup> LOx was applied to the surface of the electrode by pipet to act as the selective compound for lactate in a sample solution. A final layer of 0.6% chitosan (w/v, 75-85% deacetylated) in 0.1% (v/v) acetic acid was applied to prevent leaching of the mediator and enzyme. The biosensor was stored at 4 °C overnight before use. Results of lactate sensing without nPt and TTF are shown in Figure S6, demonstrating the lack of response in the absence of the two components. CV scans in 10× PBS were also performed after each functionalization step (Figure S7). An increase in capacitance current after platinum deposition was displayed, and two anodic oxidation peaks were observed after TTF deposition, corresponding to the formation of a TTF radical cation and a dication.<sup>53</sup> Once LOx and chitosan are applied to the surface, a reduced capacitive current is observed. Figure 4a shows the i-tcurves for the lactate biosensor in 10× PBS (0.4-1.5 mM) and an applied potential of +0.3 V. The electrons generated during the enzyme-catalyzed oxidation of lactate to pyruvate are carried to the surface of the LIG by TTF, causing an increase in current with increasing lactate concentration (shown in Figure 4a inset). 54 The LOD (3 $\sigma$  method, eq S5) was calculated as  $0.10 \pm 0.06$  mM and the sensitivity as  $33.3 \pm 0.9$  $\mu$ A mM<sup>-1</sup> cm<sup>-2</sup> in 10× PBS, similar to other LIG-based lactate biosensors.<sup>35</sup> The LOD is higher than in studies using screenprinted electrodes; however, the upper end of the dynamic range reported for these biosensors is lower, suggesting that



**Figure 5.** (a) i-t curves for potassium detection from 11 to 22 mM with a background of 10 mM K<sup>+</sup>. (b) Cumulated charge versus the logarithm of activity for potassium sensors obtained by integrating the area under the i-t curve for each current pulse ( $R^2 = 0.9908$ ). (c) i-t curves showing real-time selectivity of the potassium sensors using 15 mM Na<sup>+</sup>, Mg<sup>2+</sup>, and Ca<sup>2+</sup> as interferents. Data represents mean  $\pm$  standard deviation (n = 3).

they may be limited in monitoring higher levels of lactate such as during physical activity. 55-57 Table S2 shows a comparison of figures of merit for the nPt-LIG lactate biosensor and other recently published works. The change in current generated relative to the baseline signal for 0.4-6.2 mM lactate is shown in Figure 4b. The biosensor signal plateaus slightly above 2.5 mM lactate, demonstrating the usability of the biosensor even in conditions of relatively high lactate levels for saliva. Figure 4c shows the real-time response of the lactate biosensor to common interferents ascorbic acid (AA), uric acid (UA), and glucose, which is followed by an addition of 5 mM lactate that causes a current increase. The selectivity was further confirmed by studying the relative amount of current generated from each analyte (Figure 4d), showing that lactate generated approximately +750% change in current with the interferents (AA, UA, and glucose) and negligible change in the signal. Durability is an essential quality wearable and implantable biosensors need for use but also in general for any type of infield sensors, as the sensors may experience stress from flexing during packaging, shipping, and use. The effect of bending cycles over 3D-printed rods<sup>58</sup> of three diameters was studied for the lactate biosensors (Figure S8) with no significant difference in performance as the biosensor goes through repeat bending cycles.

**Potassium Sensor.** Constant potential coulometry is an alternative ion detection method with the potential to address limitations of traditional potentiometry including stability and reproducibility.<sup>21</sup> The method relies on a transient current flow induced by activity changes of the primary ion, which can be integrated to obtain the cumulated charge (Q).<sup>22</sup> The logarithm of the ionic activity has a linear relationship to the total cumulated charge during the current pulses. A poly(vinyl chloride) (PVC) membrane with valinomycin, a selective ionophore for potassium, was drop-coated on the surface of the nPt-LIG after treating the surface with TTF to act as the solid contact facilitating ion-to-electron transduction.<sup>59</sup> The nPt-LIG sensors were first calibrated in potentiometric mode, as shown in Figure S9, where a sensitivity of  $40.8 \pm 0.6$  mV dec<sup>-1</sup> was displayed. Figure 5a shows the raw transient current response to increasing amounts of potassium activity (11-22 mM) within the electrochemical cell. After integration, the cumulated charge was plotted versus the log activity of potassium, resulting in the linear response seen in Figure 5b. The sensitivity was calculated as  $168.2 \mu C dec^{-1}$ , displaying the usefulness of the method for detecting small changes, as evident by the large signal produced with 0.05 log step changes in potassium activity. For the lowest concentration tested (11

mM), the signal-to-noise ratio (S/N), defined as the peak signal over the standard deviation of the blank,  $^{60}$  was 193.3  $\pm$ 56.2, indicating a nearly 200 times larger signal generated for the concentration relative to the noise. Table S3 compares the figures of merit for the nPt-LIG potassium sensor with recently published electrochemical sensor reports. Results for coulometric sensing using bare LIG and LIG without nPt or TTF are shown in Figure S10, showing the lack of a response for potassium. Previous studies have established a correlation between salivary and plasma potassium levels and the usefulness of saliva as an alternative noninvasive fluid for disease diagnostics.  $^{61-63}$  The potassium levels used in this study were physiologically relevant to diagnostic levels of conditions such as type II diabetes, renal failure, and hyperthyroidism, which have shown association with salivary potassium levels. 64,65 The selectivity of the sensor was tested by using common cations found in saliva (Na+, Mg2+, and Ca<sup>2+</sup>), as shown in Figure 5c. The transient currents generated for these cations relative to the baseline were 592.8% (Ca<sup>2+</sup>), 2491.7% (Mg<sup>2+</sup>), and 623.5% (Na<sup>+</sup>) smaller than the current observed for potassium.

Pooled Saliva Analysis. Pooled human saliva samples were provided by the Research and Education in Disease Diagnostics and Intervention (REDDI) Lab at Clemson University for the analysis of the performance of both sensors in a complex solution. Samples for the lactate biosensor were diluted to 10% with 10× PBS, and samples for the potassium sensor were diluted to 10% with DI water. Calibration of the lactate biosensor was performed using the parameters mentioned above from 0.4 to 2.5 mM lactate. The biosensor displayed linear behavior within this range of concentration, as shown in Figure 6a, where the calculated sensitivity was 34.7  $\mu$ A mM<sup>-1</sup> cm<sup>-2</sup>. The potassium sensors were tested in 10% pooled saliva diluted with DI water. Calibrations were performed using the parameters discussed above from 10 to 25 mM potassium. The sensors were able to detect potassium in the complex samples (Figure 6b), as current pulses were observed for the concentrations tested. A significant reduction of the sensitivity in the pooled saliva samples was observed, as the calculated average sensitivity was 4.52  $\mu$ C dec<sup>-1</sup>. This could be due to interference from ions and metabolites present in the saliva samples. Nevertheless, both sensors were able to detect the respective analyte in pooled human saliva samples at levels relevant to sports medicine and clinical diagnostics. 14,66 To further improve the platform into an actual point-of-care salivary biosensor, future studies should focus on optimizing enzyme and ionophore deposition, sensing conditions, and

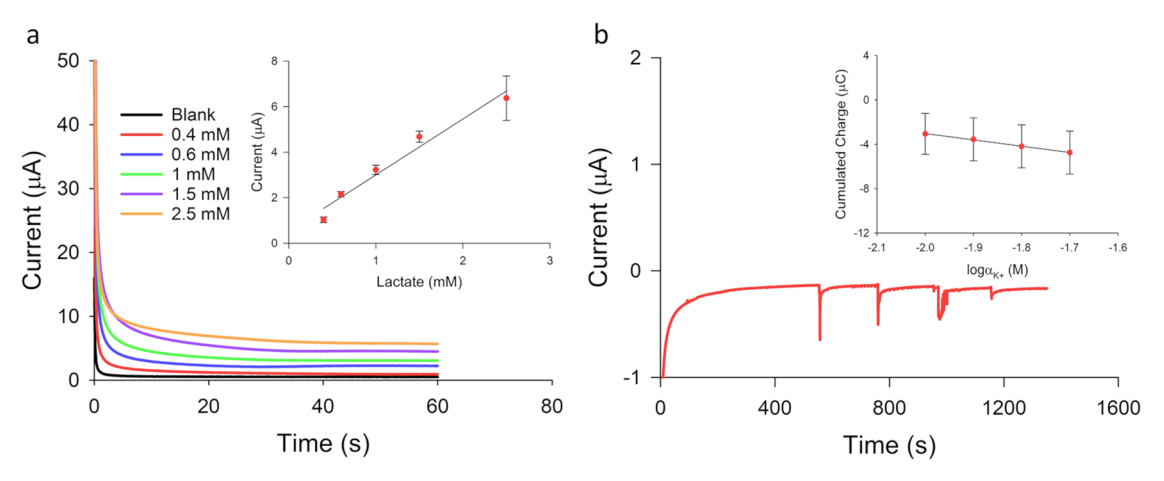


**Figure 6.** (a) Amperometric i-t curves for lactate sensing in 10% pooled saliva diluted with PBS from 0.4 to 2.5 mM lactate and the linear calibration plot (inset,  $R^2 = 0.9653$ ). (b) Current response versus the logarithm of activity for potassium (10–25 mM) sensors in 10% pooled saliva diluted with DI water. The cumulated charge (inset,  $R^2 = 0.9341$ ) was obtained by integrating the area under the i-t curve for each current pulse. Data represents mean  $\pm$  standard deviation (n = 3).

sample preparation. Properties of the LIG including mechanical durability, biocompatibility, and potential for biofouling will also need a thorough investigation to ascertain the ability of LIG to act as a wearable or implantable salivary diagnostic device. The testing of various mediators may also prove beneficial and could improve the sensitivity of both sensors.

#### CONCLUSIONS

Saliva is a favorable biological fluid for noninvasive sensing for a wide range of analytes related to health diagnostics and athletic performance. Lactate, a metabolic waste product, and potassium, an abundant electrolyte, are two analytes with associations with hydration, disease diagnostics, and fatigue levels. In this study, a one-step reagent-free laser induction process that circumvents the need for postprint annealing was used to fabricate laser-induced graphene (LIG) electrodes on a polyimide film. The LIG was covered with platinum nanoparticles (nPt-LIG) via an electroless deposition process, improving the electrical properties of the 3D porous LIG structure. The nPt-LIG electrodes were coated with a layer of the organosulfur compound tetrathiafulvalene (TTF) to act as the redox-active solid contact for the potassium sensor and as an electron carrier for the lactate biosensor. The sensors were functionalized with enzymes or ionophores for the selective monitoring of lactate and potassium, respectively, in actual pooled saliva samples. The enzymes were entrapped within a chitosan matrix to prevent leaching, and the neutral potassium ionophore, valinomycin, was dissolved in a poly(vinyl chloride) (PVC) membrane that coated the nPt-LIG structure. The lactate biosensor displayed a sensitivity of 33.3  $\pm$  0.9  $\mu$ A mM<sup>-1</sup> cm<sup>-2</sup> and a limit of detection (LOD) of  $0.10 \pm 0.06$  mM, while the potassium sensor exhibited a sensitivity of 168.2  $\mu$ C dec<sup>-1</sup> and a signal-to-noise ratio (S/N) of 193.3  $\pm$  56.2 at  $10^{-1.95}$  M potassium. Both sensors were able to detect each respective analyte at physiologically relevant levels in 10% pooled saliva samples, demonstrating the sensing capabilities in complex solutions encountered by point-of-care biosensors. The analysis time of 1 and 5 min for lactate and potassium, respectively, is significantly less than techniques performed at centralized laboratories, where samples are collected, stored, and transported, leading to results potentially taking several days. Furthermore, both sensors displayed low detection limits

and high sensitivities while showing minimal interference from other analytes commonly found in saliva, demonstrating their selectivity. The further development of salivary LIG sensors could help realize the true potential of saliva for real-time personalized healthcare monitoring and disease diagnostics and increase the understanding of mechanisms controlling saliva composition and correlations between saliva and blood composition. Improvement in point-of-care salivary biosensors could also reduce patient reliance on centralized laboratories for health analysis, potentially lead to early detection of negative health events, and improve life quality for the users. The readily modifiable surface of the nPt-LIG offers a versatile, low-cost platform to develop effective noninvasive point-ofcare biosensors for a wide range of analytes found in saliva. The nPt-LIG electrodes can be easily combined with microfluidic systems for real-time monitoring and diagnostics such as our recent work with wearable sweat sensors.

#### ASSOCIATED CONTENT

### Supporting Information

The Supporting Information is available free of charge at https://pubs.acs.org/doi/10.1021/acsanm.3c03786.

Includes all equations used; results for electroless deposition of nPt (EDS, SEM, and XPS); SEM image and Raman spectroscopy analysis of bare LIG; results for electrochemical deposition of nPt; representative Randles—Sevcik plot; CV scans after lactate biosensor functionalization; lactate and potassium response without TTF and nPt; bending studies on the lactate biosensor; representative potentiometric response of the potassium sensor; and comparison tables for the lactate and potassium sensors to current published works (PDF)

#### AUTHOR INFORMATION

#### **Corresponding Authors**

Jonathan C. Claussen — Department of Mechanical Engineering, Iowa State University, Ames, Iowa 50011, United States; orcid.org/0000-0001-7065-1077; Email: jcclauss@iastate.edu

Carmen L. Gomes — Department of Mechanical Engineering, Iowa State University, Ames, Iowa 50011, United States; orcid.org/0000-0003-0095-6478; Email: carmen@iastate.edu

#### **Authors**

Robert G. Hjort — Department of Mechanical Engineering, Iowa State University, Ames, Iowa 50011, United States; o orcid.org/0000-0003-2400-0710

Cícero C. Pola – Department of Mechanical Engineering, Iowa State University, Ames, Iowa 50011, United States

Raquel R. A. Soares — Department of Mechanical Engineering, Iowa State University, Ames, Iowa 50011, United States

Jemima Opare-Addo — Department of Chemistry, Iowa State University, Ames, Iowa 50011, United States; Ames National Laboratory, U.S. Department of Energy, Ames, Iowa 50011, United States

Emily A. Smith — Department of Chemistry, Iowa State University, Ames, Iowa 50011, United States; Ames National Laboratory, U.S. Department of Energy, Ames, Iowa 50011, United States; orcid.org/0000-0001-7438-7808

Complete contact information is available at: https://pubs.acs.org/10.1021/acsanm.3c03786

#### **Notes**

The authors declare no competing financial interest.

#### ACKNOWLEDGMENTS

The authors gratefully acknowledge funding support from the National Science Foundation under award numbers PFI-2141198 and CMMI-2037026, and the National Institute of Food and Agriculture, U.S. Department of Agriculture, award number 2018-67016-27578, awarded as a Center of Excellence, and award numbers 2020-67021-31375 and 2021-67021-34457. The authors also gratefully acknowledge Dr. Delphine Dean and the Research and Education in Disease Diagnostics and Intervention (REDDI) Lab at Clemson University for the pooled saliva samples and Dr. Curtis Mosher at the Roy J. Carver High Resolution Microscopy Facility (HRMF) at Iowa State University for the 3D microscope analysis. BioRender was used to generate components of Figure 1 and the TOC figure.

# REFERENCES

- (1) Majumder, S.; Mondal, T.; Deen, M. J. Wearable Sensors for Remote Health Monitoring. *Sensors* **2017**, *17* (1), 130.
- (2) Yoshizawa, J. M.; Schafer, C. A.; Schafer, J. J.; Farrell, J. J.; Paster, B. J.; Wong, D. T. W. Salivary Biomarkers: Toward Future Clinical and Diagnostic Utilities. *Clin. Microbiol. Rev.* **2013**, *26* (4), 781–791.
- (3) Humphrey, S. P.; Williamson, R. T. A Review of Saliva: Normal Composition, Flow, and Function. *J. Prosthet. Dent.* **2001**, 85 (2), 162–169, DOI: 10.1067/mpr.2001.113778.
- (4) Pola, C. C.; Rangnekar, S. V.; Sheets, R.; Szydłowska, B. M.; Downing, J. R.; Parate, K. W.; Wallace, S. G.; Tsai, D.; Hersam, M. C.; Gomes, C. L.; Claussen, J. C. Aerosol-Jet-Printed Graphene Electrochemical Immunosensors for Rapid and Label-Free Detection of SARS-CoV-2 in Saliva. 2D Mater. 2022, 9 (3), No. 035016, DOI: 10.1088/2053-1583/ac7339.
- (5) Rabinowitz, J. D.; Enerbäck, S. Lactate: The Ugly Duckling of Energy Metabolism. *Nat. Metab.* **2020**, 2 (7), 566–571.
- (6) Yao, Y.; Li, H.; Wang, D.; Liu, C.; Zhang, C. An Electrochemiluminescence Cloth-Based Biosensor with Smartphone-Based Imaging for Detection of Lactate in Saliva. *Analyst* **2017**, *142* (19), 3715–3724.
- (7) Yan, P.; Qin, C.; Yan, Z.; Chen, C.; Zhang, F. Can Salivary Lactate Be Used as an Anaerobic Biomarker? *PeerJ* **2023**, *11*, No. e15274, DOI: 10.7717/peerj.15274.

- (8) Spehar-Délèze, A.-M.; Anastasova, S.; Vadgama, P. Monitoring of Lactate in Interstitial Fluid, Saliva and Sweat by Electrochemical Biosensor: The Uncertainties of Biological Interpretation. *Chemosensors* **2021**, *9* (8), 195 DOI: 10.3390/chemosensors9080195.
- (9) Bocanegra, O. L.; Diaz, M. M.; Teixeira, R. R.; Soares, S. S.; Espindola, F. S. Determination of the Lactate Threshold by Means of Salivary Biomarkers: Chromogranin A as Novel Marker of Exercise Intensity. *Eur. J. Appl. Physiol.* **2012**, *112* (9), 3195–3203.
- (10) He, F. J.; MacGregor, G. A. Beneficial Effects of Potassium on Human Health. *Physiol. Plant.* **2008**, 133 (4), 725–735, DOI: 10.1111/j.1399-3054.2007.01033.x.
- (11) He, F. J.; MacGregor, G. A. Beneficial Effects of Potassium. *BMJ* **2001**, 323, 497–501, DOI: 10.1136/bmj.323.7311.497.
- (12) Lu, Y. P.; Huang, J. W.; Lee, I. N.; Weng, R. C.; Lin, M. Y.; Yang, J. T.; Lin, C. T. A Portable System to Monitor Saliva Conductivity for Dehydration Diagnosis and Kidney Healthcare. *Sci. Rep.* **2019**, 9 (1), No. 14771, DOI: 10.1038/s41598-019-51463-8.
- (13) Bilancio, G.; Cavallo, P.; Lombardi, C.; Guarino, E.; Cozza, V.; Giordano, F.; Palladino, G.; Cirillo, M. Saliva for Assessing Creatinine, Uric Acid, and Potassium in Nephropathic Patients. *BMC Nephrol.* **2019**, *20* (1), No. 242, DOI: 10.1186/s12882-019-1437-4.
- (14) Chicharro, J. L.; Lucía, A.; Pérez, M.; Vaquero, A. F.; Ureña, R. Saliva composition and exercise. *Sports Med.* **1998**, *26* (1), 17–27, DOI: 10.2165/00007256-199826010-00002.
- (15) Rattu, G.; Khansili, N.; Maurya, V. K.; Krishna, P. M. Lactate Detection Sensors for Food, Clinical and Biological Applications: A Review. *Environ. Chem. Lett.* **2021**, *19* (2), 1135–1152.
- (16) Lindner, E.; Gyurcsányi, R. E. Quality Control Criteria for Solid-Contact, Solvent Polymeric Membrane Ion-Selective Electrodes. *J. Solid State Electrochem.* **2009**, *13* (1), 51–68.
- (17) Lim, H. R.; Lee, S. M.; Park, S.; Choi, C.; Kim, H.; Kim, J.; Mahmood, M.; Lee, Y.; Kim, J. H.; Yeo, W. H. Smart Bioelectronic Pacifier for Real-Time Continuous Monitoring of Salivary Electrolytes. *Biosens. Bioelectron.* **2022**, 210, 114329 DOI: 10.1016/j.bios.2022.114329.
- (18) Chen, Y.; Bhadra, S. In A Flexible Printed Potentiometric Sensor for Potassium Ion Sensing, IEEE International Conference on Flexible and Printable Sensors and Systems (FLEPS); 2021; pp 1–4 DOI: 10.1109/FLEPS51544.2021.9469790.
- (19) Lim, H. R.; Lee, S. M.; Mahmood, M.; Kwon, S.; Kim, Y. S.; Lee, Y.; Yeo, W. H. Development of Flexible Ion-Selective Electrodes for Saliva Sodium Detection. *Sensors* **2021**, *21* (5), No. 1642, DOI: 10.3390/s21051642.
- (20) Hu, J.; Stein, A.; Bühlmann, P. Rational Design of All-Solid-State Ion-Selective Electrodes and Reference Electrodes. *TrAC, Trends Anal. Chem.* **2016**, 76, 102–114, DOI: 10.1016/j.trac.2015.11.004.
- (21) Hupa, E.; Vanamo, U.; Bobacka, J. Novel Ion-to-Electron Transduction Principle for Solid-Contact ISEs. *Electroanalysis* **2015**, 27 (3), 591–594.
- (22) Vanamo, U.; Hupa, E.; Yrjänä, V.; Bobacka, J. New Signal Readout Principle for Solid-Contact Ion-Selective Electrodes. *Anal. Chem.* **2016**, 88 (8), 4369–4374.
- (23) Balandin, A. A. Thermal Properties of Graphene and Nanostructured Carbon Materials. *Nat. Mater.* **2011**, *10*, 569–581.
- (24) Craciun, M. F.; Russo, S.; Yamamoto, M.; Tarucha, S. Tuneable Electronic Properties in Graphene. *Nano Today* **2011**, *6* (1), 42–60. (25) Kurra, N.; Jiang, Q.; Nayak, P.; Alshareef, H. N. Laser-Derived Graphene: A Three-Dimensional Printed Graphene Electrode and Its Emerging Applications. *Nano Today* **2019**, 24, 81–102.
- (26) He, Q.; Das, S. R.; Garland, N. T.; Jing, D.; Hondred, J. A.; Cargill, A. A.; Ding, S.; Karunakaran, C.; Claussen, J. C. Enabling Inkjet Printed Graphene for Ion Selective Electrodes with Postprint Thermal Annealing. *ACS Appl. Mater. Interfaces* **2017**, *9* (14), 12719–12727.
- (27) Hondred, J. A.; Stromberg, L. R.; Mosher, C. L.; Claussen, J. C. High-Resolution Graphene Films for Electrochemical Sensing via Inkjet Maskless Lithography. *ACS Nano* **2017**, *11* (10), 9836–9845.

- (28) Lin, J.; Peng, Z.; Liu, Y.; Ruiz-Zepeda, F.; Ye, R.; Samuel, E. L.; Yacaman, M. J.; Yakobson, B. I.; Tour, J. M. Laser-Induced Porous Graphene Films from Commercial Polymers. *Nat. Commun.* **2014**, *5* (1), No. 5714, DOI: 10.1038/ncomms6714.
- (29) Hjort, R. G.; Soares, R. R. A.; Li, J.; Jing, D.; Hartfiel, L.; Chen, B.; Belle, B. Van.; Soupir, M.; Smith, E.; Mclamore, E.; Claussen, J. C.; Gomes, C. L. Hydrophobic Laser Induced Graphene Potentiometric Ion Selective Electrodes for Nitrate Sensing. *Microchim. Acta* 2022, 189, 122.
- (30) Chen, B.; Johnson, Z. T.; Sanborn, D.; Hjort, R. G.; Garland, N. T.; Soares, R. R. A.; Van Belle, B.; Jared, N.; Li, J.; Jing, D.; Smith, E. A.; Gomes, C. L.; Claussen, J. C. Tuning the Structure, Conductivity, and Wettability of Laser-Induced Graphene for Multiplexed Open Microfluidic Environmental Biosensing and Energy Storage Devices. ACS Nano 2022, 16 (1), 15–28.
- (31) Garland, N. T.; McLamore, E. S.; Cavallaro, N. D.; Mendivelso-Perez, D.; Smith, E. A.; Jing, D.; Claussen, J. C. Flexible Laser-Induced Graphene for Nitrogen Sensing in Soil. ACS Appl. Mater. Interfaces 2018, 10 (45), 39124–39133.
- (32) Soares, R. R.; Hjort, R. G.; Pola, C. C.; Parate, K.; Reis, E. L.; Soares, N. F.; McLamore, E. S.; Claussen, J. C.; Gomes, C. L. Laser-Induced Graphene Electrochemical Immunosensors for Rapid and Label-Free Monitoring of Salmonella Enterica in Chicken Broth. ACS Sens. 2020, 5 (7), 1900–1911.
- (33) Yang, Y.; Song, Y.; Bo, X.; Min, J.; Pak, O. S.; Zhu, L.; Wang, M.; Tu, J.; Kogan, A.; Zhang, H.; Hsiai, T. K.; Li, Z.; Gao, W. A Laser-Engraved Wearable Sensor for Sensitive Detection of Uric Acid and Tyrosine in Sweat. *Nat. Biotechnol.* **2020**, *38* (2), 217–224.
- (34) Kucherenko, I. S.; Sanborn, D.; Chen, B.; Garland, N.; Serhan, M.; Forzani, E.; Gomes, C.; Claussen, J. C. Ion-Selective Sensors Based on Laser-Induced Graphene for Evaluating Human Hydration Levels Using Urine Samples. *Adv. Mater. Technol.* **2020**, 5 (6), No. 1901037, DOI: 10.1002/admt.201901037.
- (35) Madden, J.; Vaughan, E.; Thompson, M.; O' Riordan, A.; Galvin, P.; Iacopino, D.; Rodrigues Teixeira, S. Electrochemical Sensor for Enzymatic Lactate Detection Based on Laser-Scribed Graphitic Carbon Modified with Platinum, Chitosan and Lactate Oxidase. *Talanta* 2022, 246, No. 123492.
- (36) Claussen, J. C.; Daniele, M. A.; Geder, J.; Pruessner, M.; Mäkinen, A. J.; Melde, B. J.; Twigg, M.; Verbarg, J. M.; Medintz, I. L. Platinum-Paper Micromotors: An Urchin-like Nanohybrid Catalyst for Green Monopropellant Bubble-Thrusters. *ACS Appl. Mater. Interfaces* **2014**, *6* (20), 17837–17847.
- (37) Tékus, É.; Kaj, M.; Szabó, E.; Szénási, N. L.; Kerepesi, I.; Figler, M.; Gábriel, R.; Wilhelm, M. Comparison of Blood and Saliva Lactate Level after Maximum Intensity Exercise. *Acta Biol. Hung.* **2012**, *63* (Supplement 1), 89–98, DOI: 10.1556/ABiol.63.2012.Suppl.1.9.
- (38) Welch, C. M.; Compton, R. G. The Use of Nanoparticles in Electroanalysis: A Review. *Anal. Bioanal. Chem.* **2006**, 384, 601–619. (39) Chen, A.; Holt-Hindle, P. Platinum-Based Nanostructured
- Materials: Synthesis, Properties, and Applications. *Chem. Rev.* **2010**, 110 (6), 3767–3804.
- (40) Muzyka, K.; Xu, G. Laser-induced Graphene in Facts, Numbers, and Notes in View of Electroanalytical Applications: A Review. *Electroanalysis* **2022**, 34 (4), 574–589.
- (41) Soares, R. R.; Hjort, R. G.; Pola, C. C.; Jing, D.; Cecon, V. S.; Claussen, J. C.; Gomes, C. L. Ion-Selective Electrodes Based on Laser-Induced Graphene as an Alternative Method for Nitrite Monitoring. *Microchim. Acta.* **2023**, *190* (1), 43 DOI: 10.1007/s00604-022-05615-000604-022-000604-022-000604-022-000604-022-000604-022-000604-022-000604-022-000604-022-000604-022-000604-022-000604-022-000604-022-000604-022-000604-022-000604-022-000604-022-000604-022-000604-020-000604-000604-000604-000604-000604-000604-000604-0000604-000604-000604-000604-000604-000604-000604-0000604-000604-00
- (42) Peuckert, M.; Coenen, F. P.; Bonzel, I.-L. P. XPS Study of the Electrochemical Surface Oxidation of Platinum in N H<sub>2</sub>SO<sub>4</sub> Acid Electrolyte. *Electrochim. Acta* 1984, 29 (10), 1305–1314.
- (43) Siburian, R.; Ali, A. M.; Sebayang, K.; Supeno, M.; Tarigan, K.; Simanjuntak, C.; Aritonang, S. P.; Hutagalung, F. The Loading Effect of Pt Clusters on Pt/Graphene Nano Sheets Catalysts. *Sci. Rep.* **2021**, *11*, No. 2532.

- (44) Donev, E. U.; Hastings, J. T. Electron-Beam-Induced Deposition of Platinum from a Liquid Precursor. *Nano Lett.* **2009**, 9 (7), 2715–2718.
- (45) Huang, X.; Zhu, Y.; Kianfar, E. Nano Biosensors: Properties, Applications and Electrochemical Techniques. *J. Mater. Res. Technol.* **2021**, *12*, 1649–1672.
- (46) Elgrishi, N.; Rountree, K. J.; McCarthy, B. D.; Rountree, E. S.; Eisenhart, T. T.; Dempsey, J. L. A Practical Beginner's Guide to Cyclic Voltammetry. *J. Chem. Educ.* **2018**, 95 (2), 197–206.
- (47) Bard, A. J.; Faulkner, L. R. Electrochemical Methods: Fundamentals and Applications, 2nd ed.; John Wiley & Sons, 2000.
- (48) Nayak, P.; Kurra, N.; Xia, C.; Alshareef, H. N. Highly Efficient Laser Scribed Graphene Electrodes for On-Chip Electrochemical Sensing Applications. *Adv. Electron. Mater.* **2016**, 2 (10), No. 1600185, DOI: 10.1002/aelm.201600185.
- (49) Fenzl, C.; Nayak, P.; Hirsch, T.; Wolfbeis, O. S.; Alshareef, H. N.; Baeumner, A. J. Laser-Scribed Graphene Electrodes for Aptamer-Based Biosensing. ACS Sens. 2017, 2 (5), 616–620.
- (50) Griffiths, K.; Dale, C.; Hedley, J.; Kowal, M. D.; Kaner, R. B.; Keegan, N. Laser-Scribed Graphene Presents an Opportunity to Print a New Generation of Disposable Electrochemical Sensors. *Nanoscale* **2014**, *6* (22), 13613–13622.
- (51) Lin, J.; Peng, Z.; Liu, Y.; Ruiz-Zepeda, F.; Ye, R.; Samuel, E. L. G.; Yacaman, M. J.; Yakobson, B. I.; Tour, J. M. Laser-Induced Porous Graphene Films from Commercial Polymers. *Nat. Commun.* **2014**, *S*, No. 5714
- (52) Bandodkar, A. J.; Gutruf, P.; Choi, J.; Lee, K.; Sekine, Y.; Reeder, J. T.; Jeang, W. J.; Aranyosi, A. J.; Lee, S. P.; Model, J. B.; Ghaffari, R.; Su, C.-J.; Leshock, J. P.; Ray, T.; Verrillo, A.; Thomas, K.; Krishnamurthi, V.; Han, S.; Kim, J.; Krishnan, S.; Hang, T.; Rogers, J. A. Battery-Free, Skin-Interfaced Microfluidic/Electronic Systems for Simultaneous Electrochemical, Colorimetric, and Volumetric Analysis of Sweat. *Sci. Adv.* **2019**, 5, No. eaav3294, DOI: 10.1126/sciadv.aav3294.
- (53) Bryce, M. R.; Devonport, W.; Goldenberg, L. M.; Wang, C. Macromolecular Tetrathiafulvalene Chemistry. *Chem. Commun.* **1998**, 945–952.
- (54) Kucherenko, I. S.; Topolnikova, Y. V.; Soldatkin, O. O. Advances in the Biosensors for Lactate and Pyruvate Detection for Medical Applications: A Review. *TrAC, Trends Anal. Chem.* **2019**, *110*, 160–172, DOI: 10.1016/j.trac.2018.11.004.
- (55) Liu, J.; Zhang, L.; Fu, C. Os-Complex-Based Amperometric Bienzyme Biosensor for Continuous Determination of Lactate in Saliva. *Anal. Methods* **2015**, *7* (15), 6158–6164.
- (56) Petropoulos, K.; Piermarini, S.; Bernardini, S.; Palleschi, G.; Moscone, D. Development of a Disposable Biosensor for Lactate Monitoring in Saliva. *Sens. Actuators, B* **2016**, 237, 8–15, DOI: 10.1016/j.snb.2016.06.068.
- (57) Cunha-Silva, H.; Arcos-Martinez, M. J. Dual Range Lactate Oxidase-Based Screen Printed Amperometric Biosensor for Analysis of Lactate in Diversified Samples. *Talanta* **2018**, *188*, *779*–*787*.
- (58) Parate, K.; Rangnekar, S. V.; Jing, D.; Mendivelso-Perez, D. L.; Ding, S.; Secor, E. B.; Smith, E. A.; Hostetter, J. M.; Hersam, M. C.; Claussen, J. C. Aerosol-Jet-Printed Graphene Immunosensor for Label-Free Cytokine Monitoring in Serum. *ACS Appl. Mater. Interfaces* **2020**, *12* (7), 8592–8603.
- (59) Jarolímová, Z.; Han, T.; Mattinen, U.; Bobacka, J.; Bakker, E. Capacitive Model for Coulometric Readout of Ion-Selective Electrodes. *Anal. Chem.* **2018**, *90* (14), 8700–8707.
- (60) Bentz, C. M.; Baudzus, L.; Krummrich, P. M. Signal to Noise Ratio (SNR) Enhancement Comparison of Impulse-, Coding- and Novel Linear-Frequency-Chirp-Based Optical Time Domain Reflectometry (OTDR) for Passive Optical Network (PON) Monitoring Based on Unique Combinations of Wavelength Selective Mirrors. *Photonics* **2014**, *1* (1), 33–46.
- (61) Bilancio, G.; Cavallo, P.; Lombardi, C.; Guarino, E.; Cozza, V.; Giordano, F.; Palladino, G.; Cirillo, M. Saliva for Assessing Creatinine, Uric Acid, and Potassium in Nephropathic Patients. *BMC Nephrol.* **2019**, 20 (1), 242.

- (62) Gonçalves, A. C.; Marson, F. A.; Mendonça, R. M.; Ribeiro, J. D.; Ribeiro, A. F.; Paschoal, I. A.; Levy, C. E. Saliva as a Potential Tool for Cystic Fibrosis Diagnosis. Diagn. Pathol. 2013, 8 (1), No. 46, DOI: 10.1186/1746-1596-8-46.
- (63) Bagalad, B. S.; Mohankumar, K. P.; Madhushankari, G. S.; Donoghue, M.; Kuberappa, P. H. Diagnostic Accuracy of Salivary Creatinine, Urea, and Potassium Levels to Assess Dialysis Need in Renal Failure Patients. Dent. Res. J. 2017, 14 (1), 13-18, DOI: 10.4103/1735-3327.201138.
- (64) Rodrigues, V. P.; Franco, M. M.; Marques, C. P. C.; De Carvalho, R. C. C.; Leite, S. A. M.; Pereira, A. L. A.; Benatti, B. B. Salivary Levels of Calcium, Phosphorus, Potassium, Albumin and Correlation with Serum Biomarkers in Hemodialysis Patients. Arch. Oral Biol. 2016, 62, 58-63, DOI: 10.1016/j.archoralbio.2015.11.016.
- (65) Shirzaiy, M.; Heidari, F.; Dalirsani, Z.; Dehghan, J. Estimation of Salivary Sodium, Potassium, Calcium, Phosphorus and Urea in Type II Diabetic Patients. Diabetes Metab. Syndr. 2015, 9 (4), 332-336, DOI: 10.1016/j.dsx.2013.02.025.
- (66) Santos, R. V.; Almeida, A. L.; Caperuto, E. C.; Martins, E.; Rosa, L. C. Effects of a 30-Km Race upon Salivary Lactate Correlation with Blood Lactate. Comp. Biochem. Physiol., Part B: Biochem. Mol. Biol. 2006, 145 (1), 114-117, DOI: 10.1016/j.cbpb.2006.07.001.
- (67) Zheng, X.; Zhang, F.; Wang, K.; Zhang, W.; Li, Y.; Sun, Y.; Sun, X.; Li, C.; Dong, B.; Wang, L.; Xu, L. Smart Biosensors and Intelligent Devices for Salivary Biomarker Detection. TrAC, Trends Anal. Chem. 2021, 140, No. 116281, DOI: 10.1016/j.trac.2021.116281.
- (68) Garland, N. T.; Schmieder, J.; Johnson, Z. T.; Hjort, R. G.; Chen, B.; Andersen, C.; Sanborn, D.; Kjeldgaard, G.; Pola, C. C.; Li, J.; Gomes, C.; Smith, E. A.; Angus, H.; Meyer, J.; Claussen, J. C. Wearable Flexible Perspiration Biosensors Using Laser-Induced Graphene and Polymeric Tape Microfluidics. ACS Appl. Mater. Interfaces 2023, 15 (32), 38201-38213.

# **□** Recommended by ACS

An Integrated Sweat Sensor for Synchronous Detection of **Multiple Atherosclerosis Biomarkers** 

Jingwei Wei, Qiang Zhang, et al.

OCTOBER 10, 2023

ANALYTICAL CHEMISTRY

READ **C** 

**Two-Dimensional Ternary Nanocomposite-Decorated** Cellulose Field Effect Transistor for Nonenzymatic Sweat **Glucose Sensing** 

Kodiadka Ayshathil Bushra, K. Sudhakara Prasad, et al.

DECEMBER 27, 2023

ACS APPLIED NANO MATERIALS

READ 2

Wearable Electrochemical Microneedle Sensors Based on the Graphene-Silver-Chitosan Nanocomposite for Real-Time **Continuous Monitoring of the Depression Biomarker Sero...** 

Lakshmi R. Panicker, Yugender Goud Kotagiri, et al.

NOVEMBER 05, 2023

ACS APPLIED NANO MATERIALS

READ **C** 

Demonstrating the Analytical Potential of a Wearable Microneedle-Based Device for Intradermal CO, Detection

Águeda Molinero-Fernandez, María Cuartero, et al.

JANUARY 04, 2024

ACS SENSORS

READ 🗹

Get More Suggestions >